

Hybrid RANS/LES employing Interface Condition with Turbulent Structure

Simon Dahlström & Lars Davidson

Department of Thermo and Fluid Dynamics
Chalmers University of Technology
SE-412 96 Göteborg, Sweden

Abstract

This paper deals with the use of a hybrid RANS/LES method. A one-equation turbulence model is used in the region from the wall and out. At a certain distance from the wall a one-equation SGS model is used. Computations have been conducted on an asymmetric diffuser, using a mesh with insufficient LES resolution in the near-wall region. In order to increase the number of tests, the majority of the computations have been conducted on just the inlet channel of the diffuser. Varying the filter width in the LES region and the extent of the RANS domain, these results show good results only when the model is shifted towards RANS. The usual hybrid RANS/LES approach with a switch from RANS to LES at a matching line does not work (a smooth transition does not help either). An additional condition seems to be required at the interface. In the second part of this paper, the use of turbulent structures from the inlet data as additional conditions at the interface are investigated. Good hybrid RANS/LES results are obtained for the inlet channel case and the diffuser.

Introduction and Motivation

Coarse LES fails to predict even simple channel flow when the Reynolds number is too high. Because of constraints on the resolution near walls, which lead to excessive computer costs, LES is not a feasible method in most practical flow situations, where accurate predictions of the boundary layer is important. If, despite the costs, a wall-resolved LES is undertaken, it gives good results in a range of flows. This has been demonstrated in simulations of the flow around the A-profile [1] or of the flow in the asymmetric diffuser [2], which is also studied in the

present paper. In a wall-resolved LES the structures close to the wall are sufficiently resolved and the success of the above mentioned simulations only stresses the importance of the near-wall region and its interaction with the outer flow. For flows where the near-wall structures play a subdominant role, compared to the outer flow structures, LES has been proven to be a good method, e.g. when predicting the massive separation around airfoils beyond stall with the DES approach [3–5] or the wake flow behind a buss [6].

The question is to what extent a well-resolved LES of the outer flow is important in *mildly separated flows or attached boundary layers*? Several studies of near-wall modelling for LES are reported in the literature. RANS has been used e.g. in Refs. [7–10] and wall-functions (such as the Werner-Wengle [11] and based on the instantaneous wall law) have been used in Refs. [12–14]. Applied to mildly separated flows or attached boundary layers, although giving better results than with no near-wall model, none of the above mentioned approaches have been successful. Turbulent structures are used as approximate boundary conditions to LES in Ref. [15] and a method called LNS where additional conditions are imposed at the interface between the RANS and LES region is used in Ref. [16]. Also LES close to the wall, RANS in the outer region [17] is interesting regarding the matching of the two methods. Interface criterias at the matching line are investigated in Ref. [18]. In this paper we aim to study the usefulness of LES in the off-near-wall region when RANS is used in the near-wall region. It is our hope that coarse LES in the outer region performs better than RANS if the near-wall region is modelled and this at an acceptable computing cost.

This paper is divided in two parts, where in the first part the models, set-up and results when the standard hybrid RANS/LES is used are presented. In the second part of this paper the new interface condition is described and results from this approach are presented.

Governing Equations & Modelling Issues

Filtering or time averaging (the bar means filtering in the LES region and time averaging in the RANS region) of the incompressible continu-

ity and momentum equations results in

$$\frac{\partial \bar{u}_i}{\partial x_i} = 0 \quad (1)$$

$$\frac{\partial \bar{u}_i}{\partial t} + \frac{\partial}{\partial x_j} (\bar{u}_i \bar{u}_j) = -\frac{1}{\rho} \frac{\partial \bar{p}}{\partial x_i} + \frac{\partial}{\partial x_j} \left[\nu \frac{\partial \bar{u}_i}{\partial x_j} - \tau_{ij} \right] \quad (2)$$

$$\tau_{ij} = \overline{u_i u_j} - \bar{u}_i \bar{u}_j \quad (3)$$

Here, τ_{ij} are the subgrid scale (SGS) or turbulence stresses. In LES they are the contribution of the small scales, the unresolved stresses. In RANS they are the contribution of all turbulence. In either case they are unknown and need to be modelled, here using the eddy-viscosity hypothesis:

$$\tau_{ij} - \frac{1}{3} \delta_{ij} \tau_{kk} = -2\nu_T \bar{S}_{ij} \quad (4)$$

Here, $\bar{S}_{ij} = \frac{1}{2} \left(\frac{\partial \bar{u}_i}{\partial x_j} + \frac{\partial \bar{u}_j}{\partial x_i} \right)$ is the strain rate (filtered in the LES sense and time averaged in the RANS sense).

The transport equation for the kinetic energy reads:

$$\frac{\partial k_T}{\partial t} + \frac{\partial}{\partial x_j} (\bar{u}_j k_T) = \frac{\partial}{\partial x_j} \left[(\nu + \nu_T) \frac{\partial k_T}{\partial x_j} \right] + P_k - C_\epsilon \frac{k_T^{3/2}}{\ell_\epsilon}$$

$$P_k = 2\nu_T \bar{S}_{ij} \bar{S}_{ij}, \quad \nu_T = C_k \ell_k k_T^{1/2} \quad (5)$$

The one-equation model used in the present computations is based on the one-equation SGS model by Yoshizawa [19] and the one-equation turbulence model by Chen and Patel [20]. In the LES region it models the kinetic energy of the unresolved stresses ($k_T = k_{sgs}$) and in the RANS region it is a model for the turbulent kinetic energy ($k_T = k$). The original model constants and length scales are summarised in Table 1.

In most of our hybrid RANS/LES computations the k -equation RANS model is switched abruptly to the SGS model at a prescribed node away from the wall (the matching line). We are able to smooth out the transition between the two models by using the model described in Appendix.

In the LES region the filter width, Δ , should be in the order of the grid size and could e.g. be chosen as the minimum or maximum side of a finite-volume cell. The filter width (SGS model) should depend

	Chen and Patel	Yoshizawa [21]
C'_ε	1	1.05
C_k	0.09	0.07
ℓ_ε	$2.495 \cdot y(1 - e^{-0.2y\sqrt{k}/\nu})$	Δ
ℓ_k	$2.495 \cdot y(1 - e^{-0.0143y\sqrt{k}/\nu})$	Δ

Table 1: The original one-equation models.

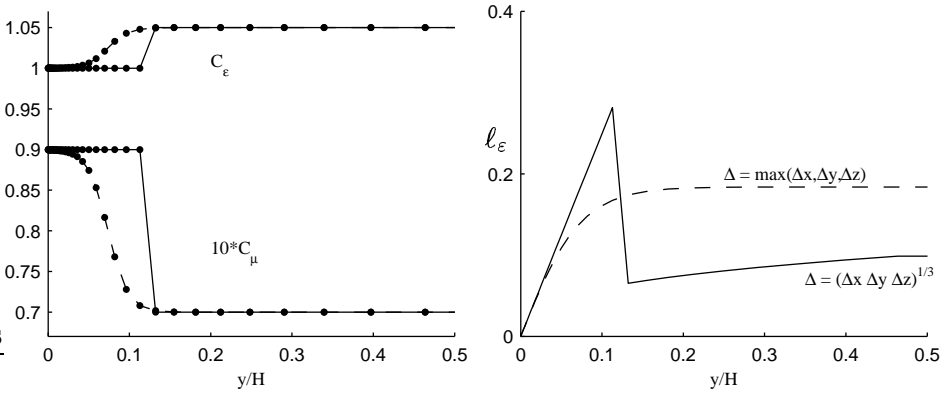


Figure 1: Two examples of the constants and length scales away from the wall at different matching lines (solid line: at $y = 0.123H$ without smoothing; dashed line: at $y = 0.074H$ with smoothing) and for different filter widths in the outer LES region.

on how fine the grid is. The choice is of less importance in a wall-resolved LES since the influence of the SGS model is small (in the limit, when the resolution is of DNS quality, the model should produce no eddy viscosity). However on a coarse mesh, the model should produce more SGS eddy viscosity in order to account for the contribution of the unresolved stresses and the influence of the model is larger. The question is how important the SGS model or choice of filter width is in the region away from the wall if the near-wall region is modelled? In our hybrid RANS/LES study and the first part of this paper different filter widths have been tested when the extent of the RANS-modelled

region has been increased. Among the filter widths tested are:

$$\begin{aligned}\Delta &= \min(\Delta x, \Delta y, \Delta z) \\ \Delta &= (\Delta x \Delta y \Delta z)^{1/3} \\ \Delta &= 2.495 \cdot y_{ml} \\ \Delta &= \max(\Delta x, \Delta y, \Delta z),\end{aligned}$$

where y_{ml} is the distance from the wall to the matching line.

Computational setup

Based on the inlet channel height, H , and the bulk velocity, U_b , the Reynolds number is 18000. The outlet channel has a height of $4.7H$ (see Fig. 2). More details about the asymmetric plane diffuser case can e.g. be found in Ref. [22].

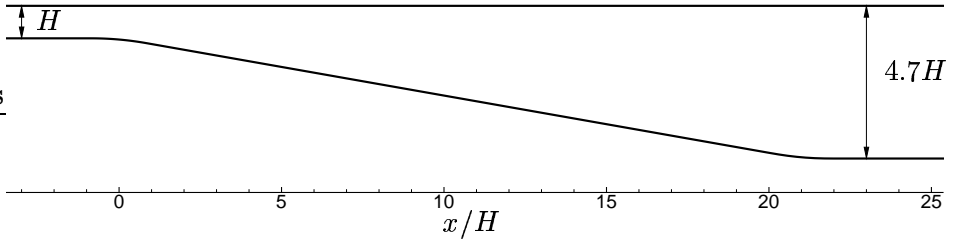


Figure 2: The diffuser case.

Mesh

We have deliberately constructed a coarse mesh (Fig. 3), with a resolution much coarser than a wall-resolved resolution (see Fig. 4). The mesh consists of 258 nodes in the streamwise direction and 66 in the wall-normal direction. In the spanwise direction 24 nodes are used and the grid size, Δz , is set to $0.184H$, which means that the extent in this direction, L_z , is equal to $4.0H$. The stretching in the wall-normal direction is 17% and the wall distance to the first node, y_1^+ , is less than 1.

56 nodes are placed in the inlet channel in the streamwise direction. As mentioned in the introduction, computations have been conducted on the inlet channel. Here the spanwise extent is decreased: using

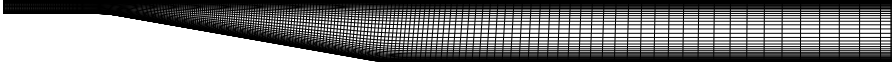


Figure 3: The diffuser mesh

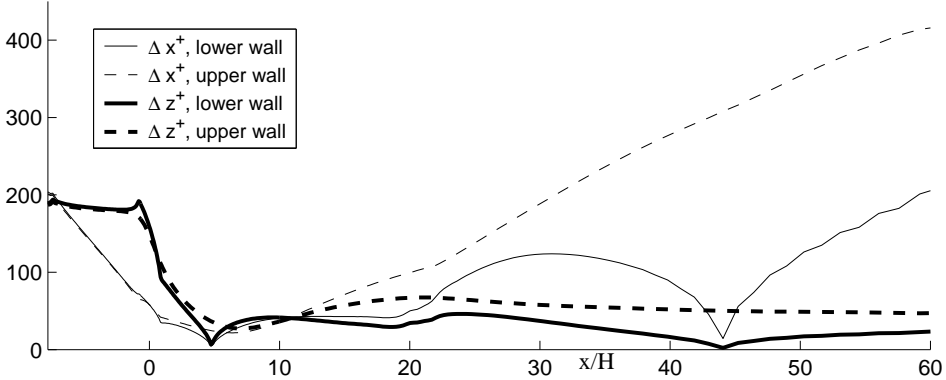


Figure 4: Resolution along the diffuser.

18 nodes and the same resolution giving $L_z = 2.94H$. Also a finer-resolution mesh is used: 24 nodes and $\Delta z = 0.061H$ ($L_z = 1.34H$). Further, a stretching of 17 and 11 % in the wall-normal direction are investigated. With these meshes we wish to study the effect of a stretching of as much as 17% and the effect of the spanwise resolution.

The inlet is located at $x = -7.9H$ and the outlet at $x = 60H$ for the diffuser and $x = -0.99H$ for the inlet channel case. Instantaneous DNS data from a channel computation at $Re_\tau = 500$ is used as inlet boundary condition. At the outlet a convective boundary condition is used for the velocities.

The time step is set to $\Delta t = 0.0441H/U_b$ (giving a maximum CFL-number of approximately one). The time averaging is started after 1 flow-through time and the data is then collected for another 2 flow-through times. For initial test computations, this amount of time is regarded as sufficient. In the inlet-channel computations an twice as fine time step is used and here the time averaging is started after 8 flow-through times and data is then collected for another 50 flow-through times.

An incompressible, finite volume code is used [8]. For space discretisation, central differencing is used for all terms. The Crank-Nicolson

scheme is used for time discretisation. The numerical procedure is based on an implicit, fractional step technique with a multigrid pressure Poisson solver and a non-staggered grid arrangement [23].

Hybrid RANS/LES results

We now turn to the results and first to those from the inlet-channel computations. It is of course a minimum requirement to have a model that works acceptable in the channel flow in order to get reliable results on the diffuser flow. Figure 5 shows velocity profiles (collected close to the outlet) for various filter widths and with different extents of the RANS region. There is little or no difference between a stretching of 11 or 17 % in the wall-normal direction. Thus results from only either one of the cases are presented. The wall distance to the first node, y_1^+ , is less than one in both cases and that is perhaps what is most important. The figure shows that we get better results the larger the extent of the RANS region is (except for the pure one-equation RANS computation).

Focusing on the spanwise resolution, the first-order statistics should preferably not change when going from finer to coarser resolution, if the SGS model does its job. We get the worst results when the smallest cell side is used as filter width and best results with $\Delta = \max(\Delta x, \Delta y, \Delta z)$ for the widest range of matching-line distances. In the fine-resolution case Δx is the largest side and in the coarse resolution case $\Delta z = 0.184H$ is the largest one. That is, this filter width is sensitive to the resolution in grid planes parallel to the wall, contrary to e.g. $\Delta = \min(\Delta x, \Delta y, \Delta z)$.

The question is how to interpret the role of the filter width in these coarse resolution cases? The resolved stresses shown in Fig. 6 are very low for the computations which agree well with the DNS data, i.e. a large part of the domain is covered by RANS. The role of the filter width in these cases seems to shift over to the role of an length-scale limiter, often used in RANS modelling, in order to set a limit on the eddy viscosity. The eddy viscosity needs to be limited in the outer parts of the boundary layer for simple one-equation RANS models [24] to decrease the production of kinetic energy. The Johnston limiter ($l_0 = 0.085\delta/C_\mu^{3/4}$) is equal to $0.259H$ ($\delta = H/2$) and this is close to the filter width $2.495y_{ml} = 0.281H$ for the case with $y_{ml}^+ \approx 110$, which gives very good velocity profile (see Fig. 5). $\Delta = \max(\Delta x, \Delta y, \Delta z)$ gives a filter width of $0.184H$ in the coarse resolution case, which is smaller than the Johnston limiter but still explains why the results are slightly better

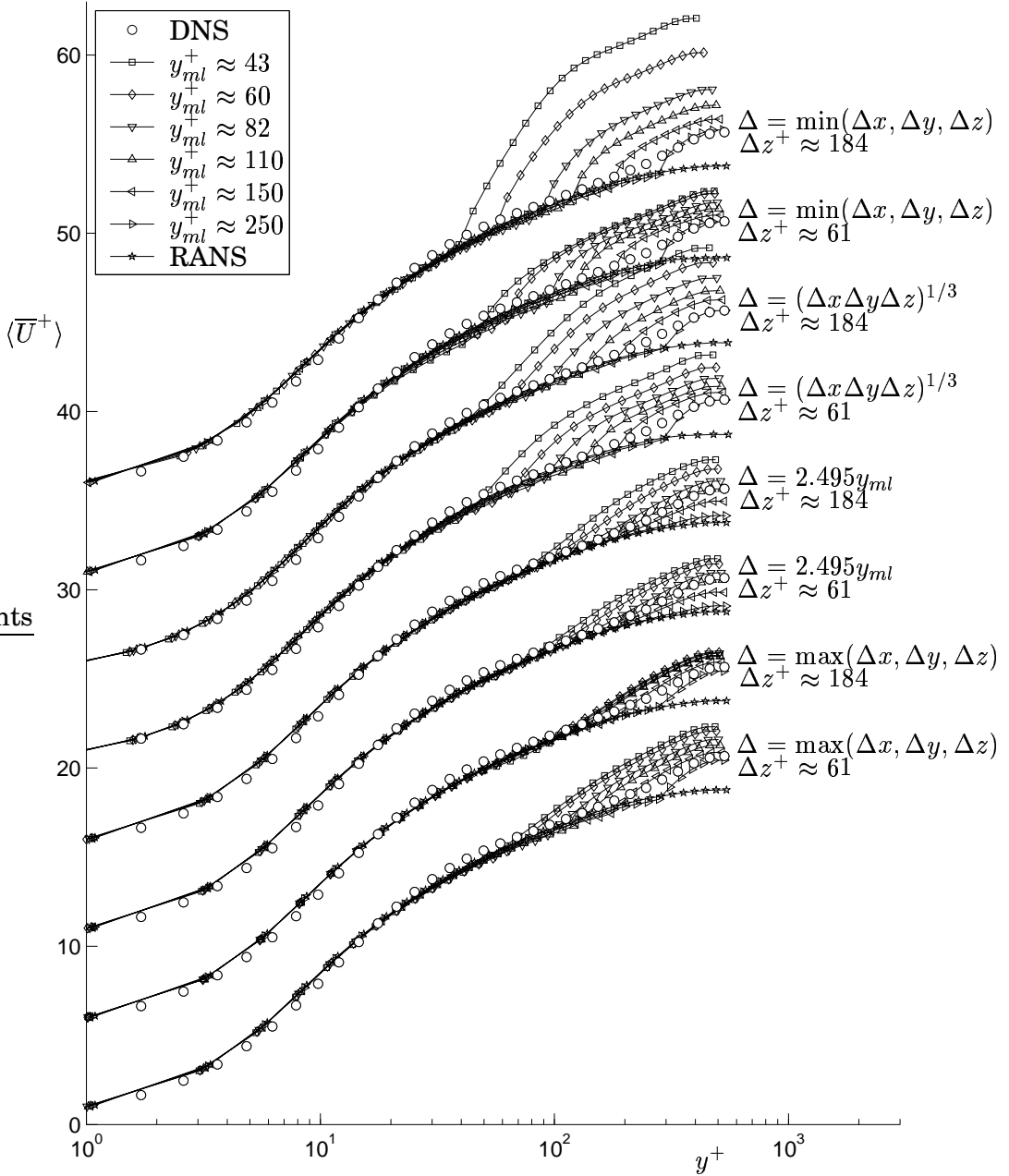


Figure 5: Velocity profiles for the inlet channel case

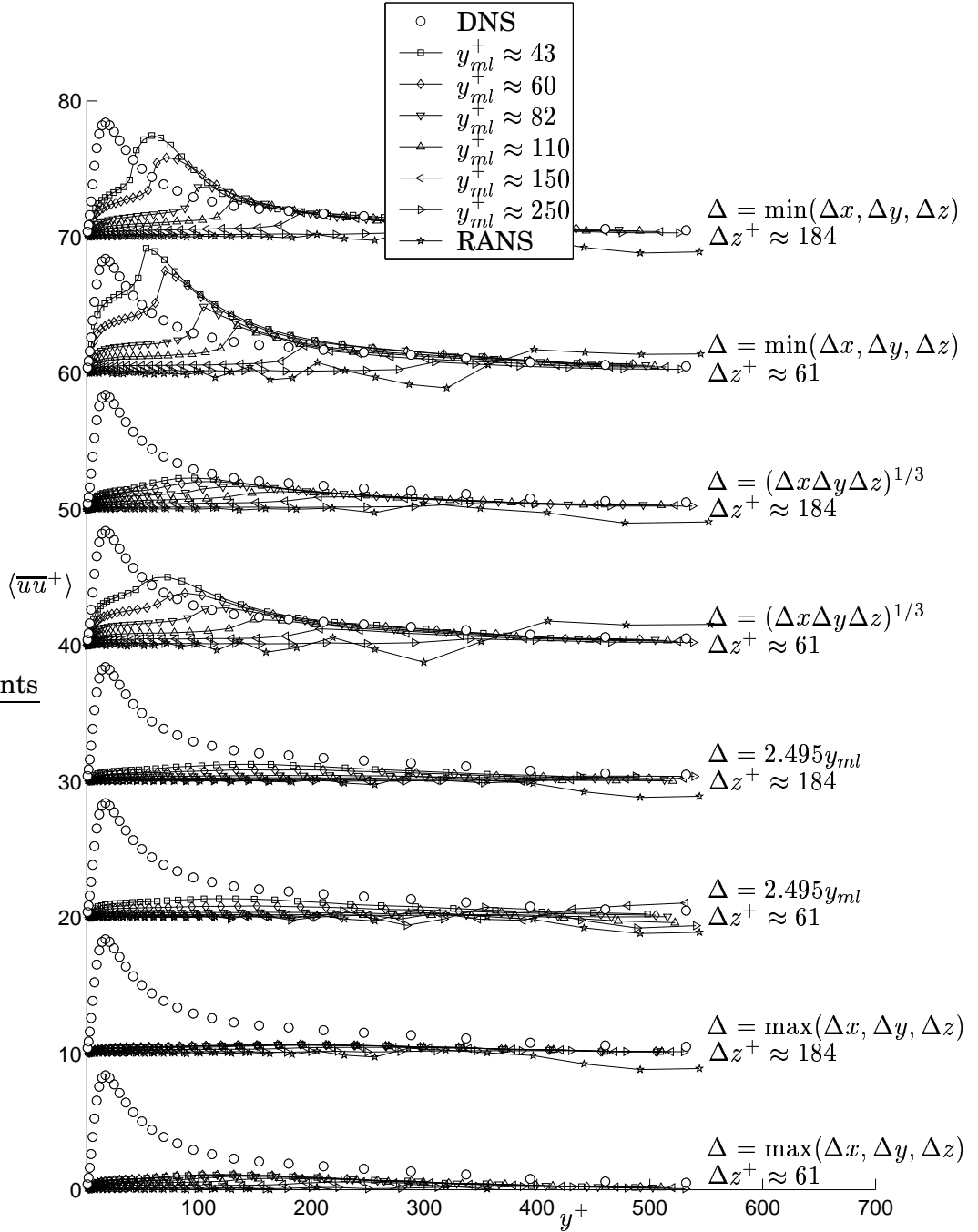


Figure 6: Resolved stress profiles for the inlet channel case

compared to the finer-resolution case, for which Δx is the largest side, where $\Delta = 0.073H$ at the outlet.

Although $\Delta = \max$ on the inlet channel gives almost no resolved stresses, this filter width has been used on the diffuser with a matching line at $y_{ml}^+ \approx 110$ at the inlet channel. Also filter widths larger than $\Delta = \max$ has been investigated, ranging up to the Johnston Eddy viscosity limiter $0.085\delta/C_\mu^{3/4}$. In Figs. 7 to 11 results from these computations are presented. The filter widths used and also shown in Fig. 7 are (in increasing order):

$$\begin{aligned}
\Delta &= \max(\Delta x, \Delta y, \Delta z) \\
\Delta &= \max(\Delta x, y_{ml}, \Delta z) \\
\Delta &= (\max(\Delta x, 2.495 \cdot y_{ml}, \Delta z) + 3 \cdot \max(\Delta x, \Delta y, \Delta z))/4 \\
\Delta &= (\max(\Delta x, 2.495 \cdot y_{ml}, \Delta z) + \max(\Delta x, \Delta y, \Delta z))/2 \\
\Delta &= (3 \cdot \max(\Delta x, 2.495 \cdot y_{ml}, \Delta z) + \max(\Delta x, \Delta y, \Delta z))/4 \\
\Delta &= \max(\Delta x, 2.495 \cdot y_{ml}, \Delta z)
\end{aligned} \tag{6}$$

The resolved stresses are too high in the inclined-wall region and downstream when $\Delta = \max$ is used (see Figs. 10 and 11) and thus also larger filter widths have been used. However, as seen in Figs. 10 and 11, the profiles shown with thicker lines are computations with practically no resolved stresses, i.e. they are close to RANS.

Looking at the velocities and the pressure and skin friction coefficients (Figs. 7 and 8) the more LES-like solutions (the thinner lines) tend to have too thick separation bubbles. This leads to too high velocities around the bubble. In the reattachment region the flow is accelerated too much (from going around the too wide bubble, to the reattachment). This is seen as the little dip in the pressure coefficient at the same place as the large dip in the skin friction. The accelerated flow then reattaches with too large momentum leading to the high peak in C_f on the lower wall. On the upper wall the velocities are too low because of continuity. Looking at the more RANS-like computations (the thicker lines), the thickness of the bubble is much better predicted. Especially in the inclined wall region the velocities are well predicted. Downstream of the inclined wall the mechanism of the reattachment is poorly captured (it is far too slow), the separation bubble being too long and the recovery length much too long. This is a usual problem for RANS models: to have a too slow redevelopment of the boundary layer downstream of the reattachment. More RANS-like results are presented in Appendix.

The eddy viscosities are shown in Fig. 9. Especially note the dif-

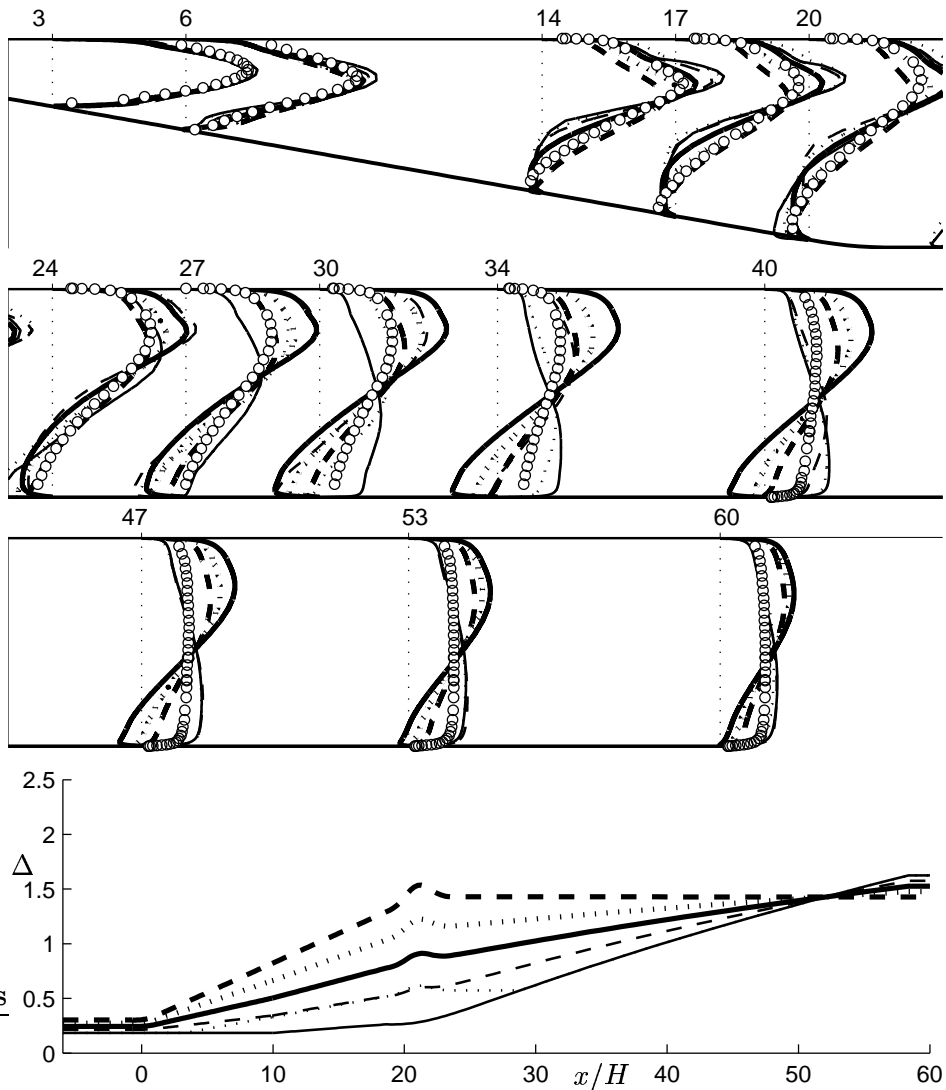


Figure 7: Diffuser flow. $\langle \bar{U} \rangle$ velocities. The difference between the computations are shown in the bottom figure, where the filter widths in the LES region are shown (for details see Eq. 6).

ference of the viscosity in the RANS region in the separation region, where the viscosity is much lower in the RANS-like computations (the thicker lines). Note that it is only the filter widths in the outer LES region that differs between the different computations.

From the computations on the inlet channel, the results from the hybrid RANS/LES approach are disappointing, giving good results only when the resolved stresses are close to zero and the filter width acts as a length-scale limiter, limiting the eddy viscosity in the outer parts of the boundary layer.

Diffuser computations show that although RANS with the eddy viscosity limiter works fine for the inlet-channel case, we get a too large separation bubble and too slow recovery of the outlet channel boundary layer. In the more LES-like simulations the redevelopment is better and the mechanism of the reattachment is better captured.

Perhaps it is important that the simulation is indeed a large-eddy simulation in the outer region, in order to take advantage of the method in more complex flow situations where the RANS approach does not work. It is not enough just using RANS in the near-wall region in order to get good results in the LES region. An additional condition is needed at the interface. Thus, in the next section we have taken a step back, looking at the inlet-channel case again, investigating a way of using turbulent structures from the inlet data as additional conditions at the interface.

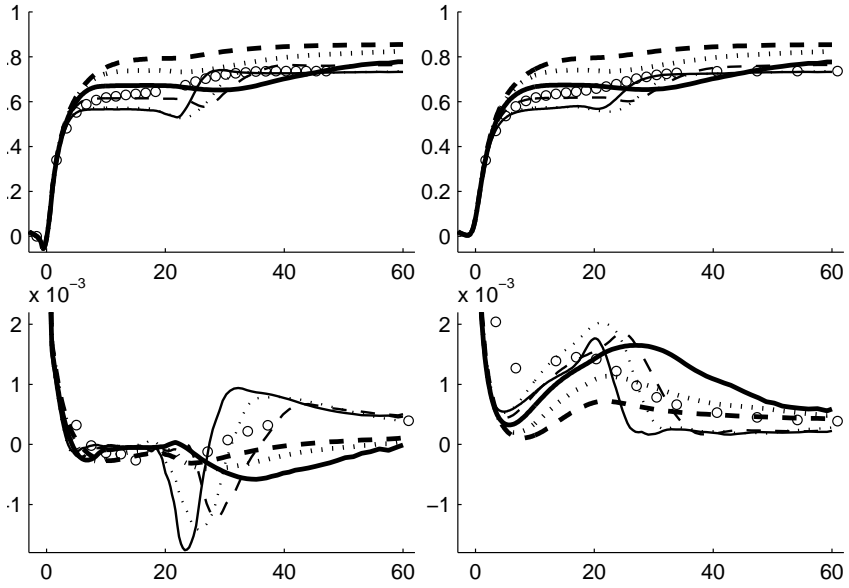


Figure 8: Diffuser flow. C_p (top figures) and C_f (figures below) on the bottom wall (left figures) and top wall (right figures). Same computations as described in Fig. 7.

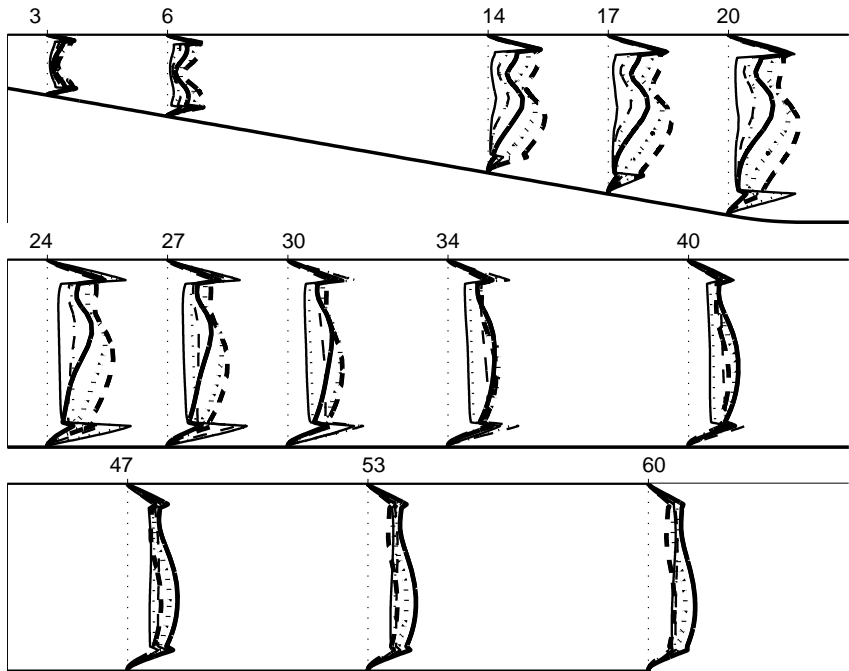


Figure 9: Diffuser flow. Viscosities ν_T/ν . Same computations as described in Fig. 7.

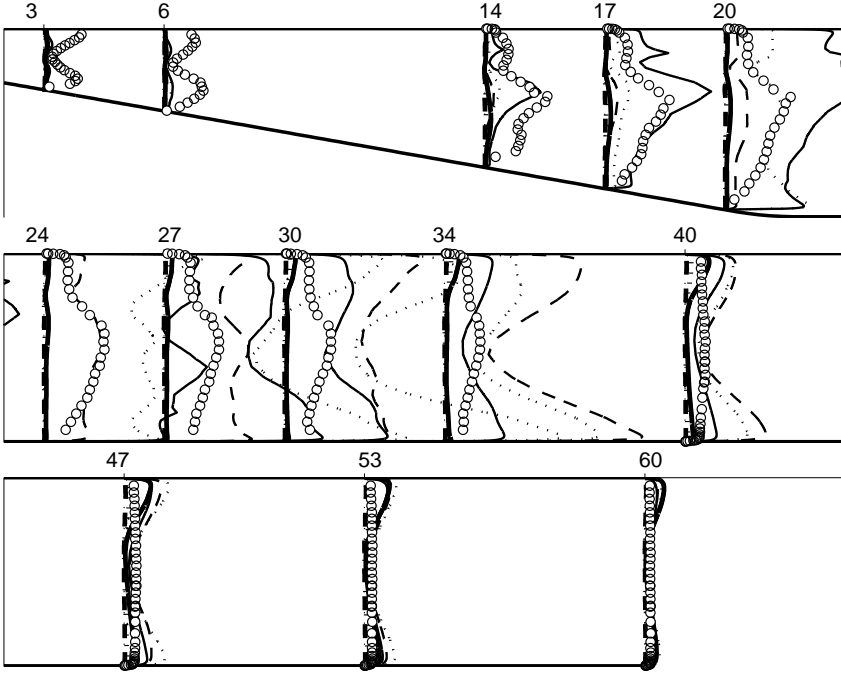


Figure 10: Diffuser flow. Resolved $\langle \overline{uu} \rangle$ stresses. Same computations as described in Fig. 7.

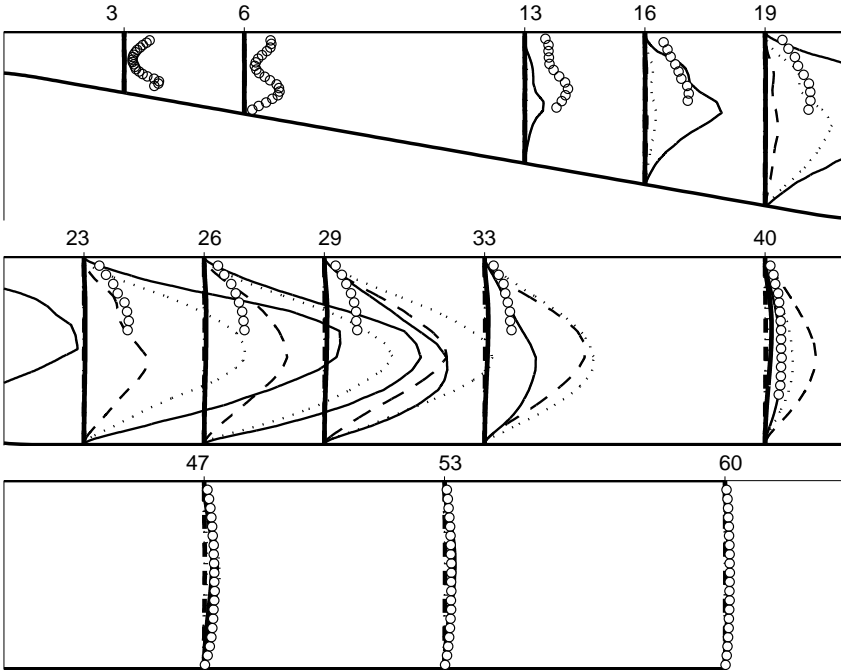


Figure 11: Diffuser flow. Resolved $\langle \overline{vv} \rangle$ stresses. Same computations as described in Fig. 7.

Hybrid RANS/LES with additional conditions at the matching region

Interface conditions

Instantaneous DNS data from a channel computation at $Re_\tau = 500$ is used as inlet boundary condition. The instantaneous DNS data, at a prescribed distance from the wall, is transformed along a matching plane at each time step using Taylor's hypothesis or the assumption of "frozen turbulence". We imagine that the DNS turbulence is frozen and just convected downstream (see Fig. 12). At each point, s_2 , at the matching plane, we can compute the travelling time, t_0 , it takes for the inlet data (at point s_1) to reach point s_2 , as

$$t_0 = - \int_{s_1}^{s_2} \frac{ds}{u_s(s)}, \quad (7)$$

where u_s is the velocity along the streamline. However, we modify the level of the turbulence by scaling it with the kinetic energy at the point, $k(s_2)$, (from the one-equation model) and the inlet kinetic energy, $k(s_1)$, (from the DNS data):

$$u'(s_2, z, t) = u'(s_1, z, t_0) \cdot \sqrt{\frac{k(s_2)}{k(s_1)}} \quad (8)$$

This is computed in the same way for the fluctuations in the other directions (v' and w'). In this way we have got an approximate tur-

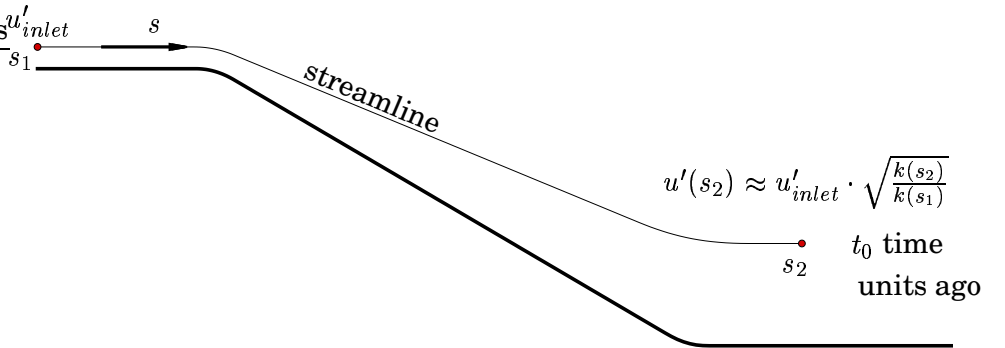


Figure 12: Interface condition using Taylor's hypothesis.

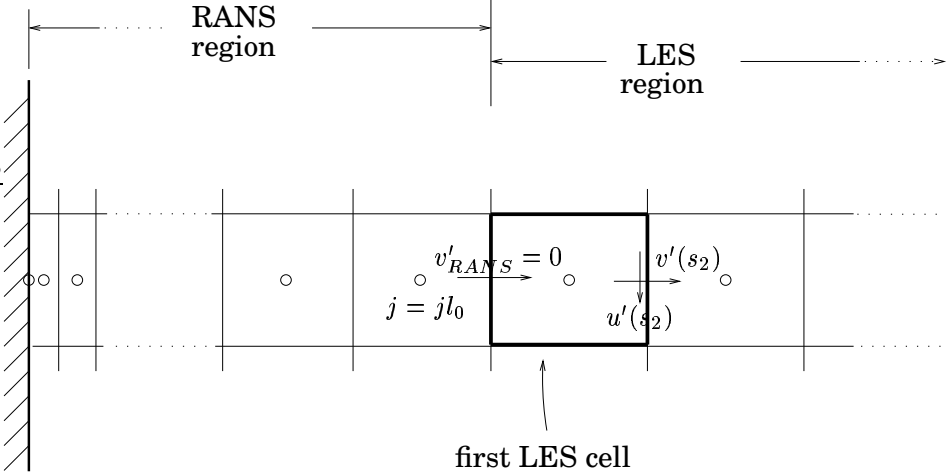


Figure 13: Interface condition.

bulent structure at the matching plane. This is implemented in the code at the first LES cell (see Fig. 13), where a source term equal to $-\partial u'_i(s_2)v'(s_2)/\partial n$, is added to the u_i -momentum equation. Here n is the coordinate from the wall into the flow.

Results

Figure 14 shows the results from the simulations of the inlet-channel flow with the interface condition described above. The coarse mesh is used, i.e. $\Delta z^+ \approx 184$. The interface region is placed at a wall distance of approximately 43 wall units. In the LES region the filter width is set to the volume of a finite-volume cell ($\Delta = (\Delta x \Delta y \Delta z)^{1/3}$). For comparison Fig. 14 also shows the results when no interface condition is used ($y_{ml}^+ \approx 43$, $\Delta = (\Delta x \Delta y \Delta z)^{1/3}$ and $\Delta z^+ \approx 184$ in Fig. 5) and the profiles for one of the RANS-like computations ($y_{ml}^+ \approx 110$, $\Delta = 2.495 y_{ml}$ and $\Delta z^+ \approx 184$ in Fig. 5). Because of the interface condition, the resolved normal and shear stresses increase in the matching region (they peak at the matching line). The resolved kinetic energy exceeds that of the DNS data and the total energy is almost twice as high as the DNS kinetic energy at the matching line. Nevertheless the velocity-profile agreement improves considerable, compared to when no interface condition is used. Looking at the eddy viscosity (the bottom figure to the right in Fig. 14), the idea with hybrid RANS/LES is illustrated: when reaching the LES region, the eddy viscosity decreases significantly and

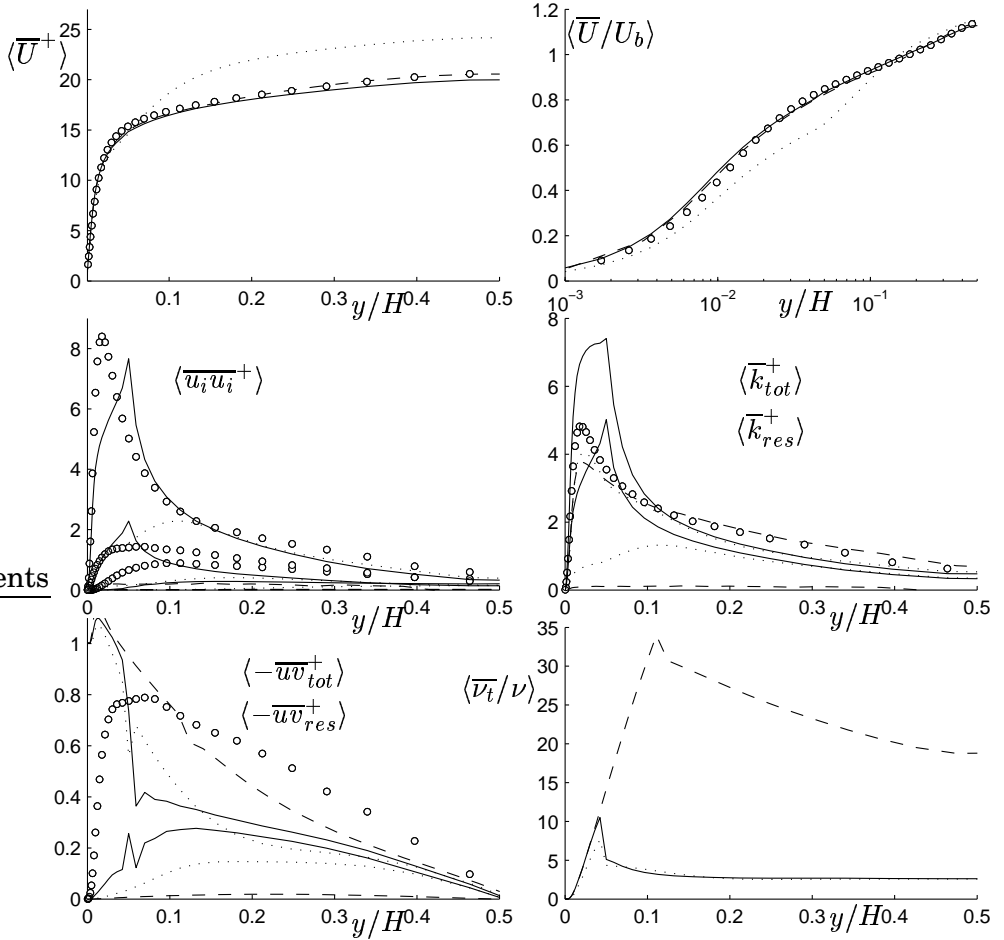


Figure 14: Profiles for the inlet channel case. Dashed lines: RANS-like computation; dotted lines: hybrid RANS/LES without interface conditions at $y_{ml}^+ \approx 43$; solid lines: hybrid RANS/LES with interface conditions at $y_{ml}^+ \approx 43$.

thus the modelled shear stress ($\overline{uv}_{tot}^+ - \overline{uv}_{res}^+$) becomes low (see bottom figure to the left), resulting in that the resolved stresses increase. In Fig. 15 the matching line is varied and set to $y_{ml}^+ \approx 82$. The velocity profiles show only slight disagreement and the interface condition seems to be quite insensitive to the choice of matching-line location.

The results from the simulations with the interface condition applied on the diffuser flow are shown in Figs. 16-22. Here the solid lines

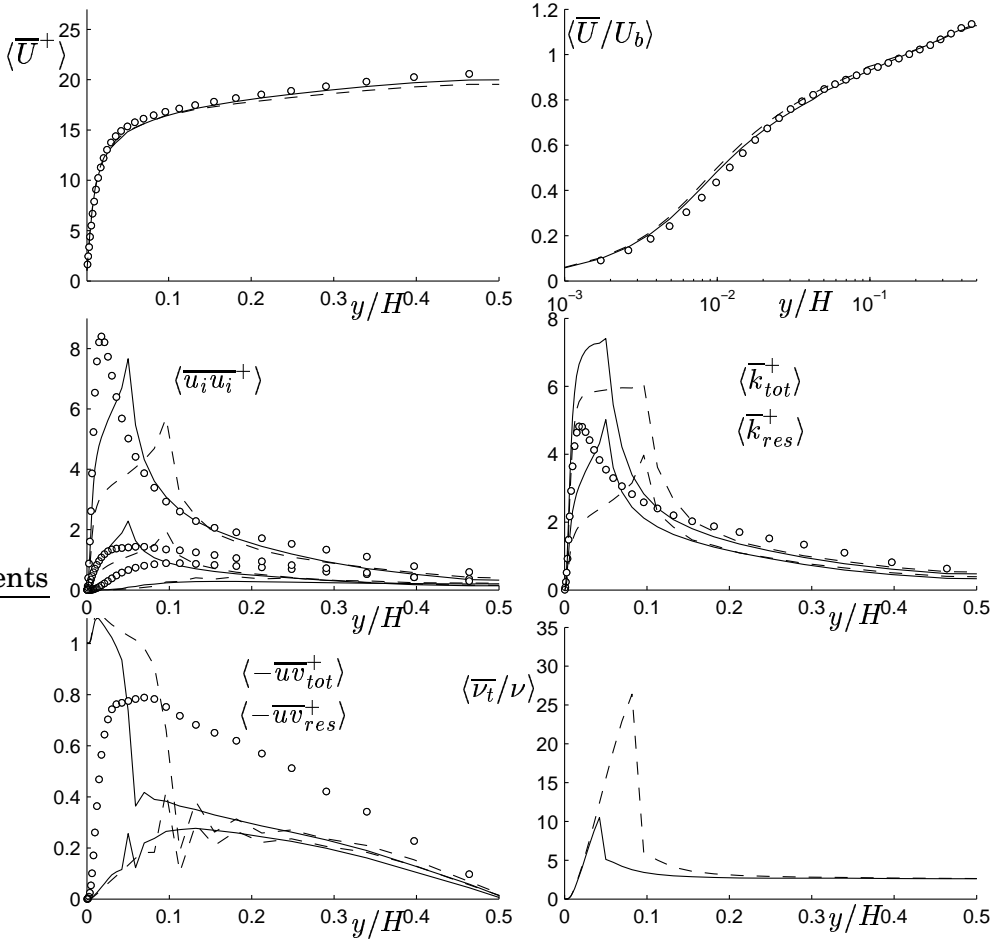


Figure 15: Variation of the matching line region in the inlet channel case. Hybrid RANS/LES profiles with interface condition at $y_{ml}^+ \approx 43$ (solid lines) and at $y_{ml}^+ \approx 82$ (dashed lines).

are results from the new approach and the dashed lines are results from one of the best RANS-like computations, presented in the previous section. Streamlines are shown in Fig. 16 for the hybrid RANS/LES approach and the figure shows that the simulation is instationary in the LES region. The matching region for the hybrid RANS/LES approach is at $y_{ml}^+ \approx 43$. This value is at the inlet channel. Downstream, the RANS region is within a constant mass flow (so that the stream-wise mass flow in the RANS region is constant for all x). The pressure

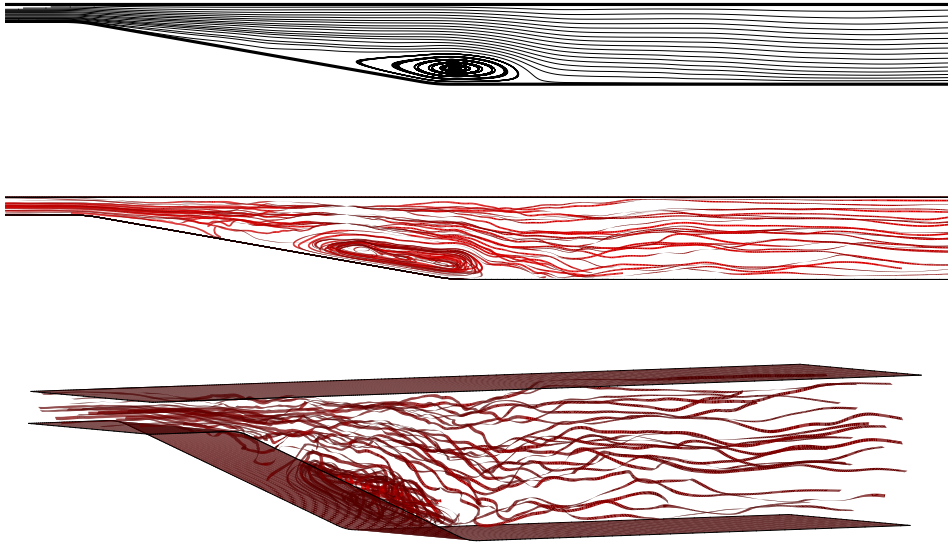


Figure 16: Streamlines, time averaged and instantaneous, in 2D and 3D views, from the hybrid RANS/LES simulation with turbulent interface condition.

and skin friction coefficients are shown in Fig. 17. The skin friction coefficient is reasonably well predicted for the hybrid RANS/LES computation, however the level for the pressure coefficient is too high in the diffuser. In Fig. 18 velocity profiles are shown and compared to experiments. In the RANS computation we get good results in the inlet channel and in the inclined wall region, however the separation bubble is too large and there is a too slow redevelopment of the outlet channel boundary layer. The hybrid RANS/LES simulation gives good results all along the diffuser and the length of the separation bubble is close to the length measured in the experiments. The total shear stresses (resolved plus modelled) are shown in Fig. 19. The RANS-like computation shows good agreement with the experiments. The eddy viscosities are shown in Fig. 20, note how the RANS region extends far from the wall in the separated-flow region because of the mass flow condition for the matching line. The resolved normal stresses in the streamwise and wall-normal directions are shown in Figs. 21 and 22 respectively. The stresses are low in the RANS region for the hybrid approach, especially

in the separated region.

Conclusions & Ongoing Work

For the inlet-channel computations, the results from the standard hybrid RANS/LES approach are disappointing, giving good results only when the resolved stresses are close to zero and the filter width acts as a length-scale limiter, limiting the eddy viscosity in the outer parts of the boundary layer.

Diffuser computations show that although RANS with the eddy viscosity limiter works fine for the inlet-channel case, we get a too large separation bubble and too slow recovery of the outlet channel boundary layer. In the more LES-like simulations the redevelopment is better and the mechanism of the reattachment is better captured.

The results for the hybrid RANS/LES approach using turbulent structures are promising. The inlet-channel results are good and seem to be independent of the choice of matching line. Good results are also obtained for the diffuser flow. In future work still more tests will be conducted on the diffuser and the approach will also be applied on the flow around the Aerospatiale A-profile.

Acknowledgements

This work was financed by the FLOMANIA project (Flow Physics Modelling - An Integrated Approach) is a collaboration between Alenia, AEA, Bombardier, Dassault, EADS-CASA, EADS-Military Aircraft, EDF, NUMECA, DLR, FOI, IMFT, ONERA, Chalmers University, Imperial College, TU Berlin, UMIST and St. Petersburg State University. The project is funded by the European Union and administrated by the CEC, Research Directorate-General, Growth Programme, under Contract No. G4RD-CT2001-00613.

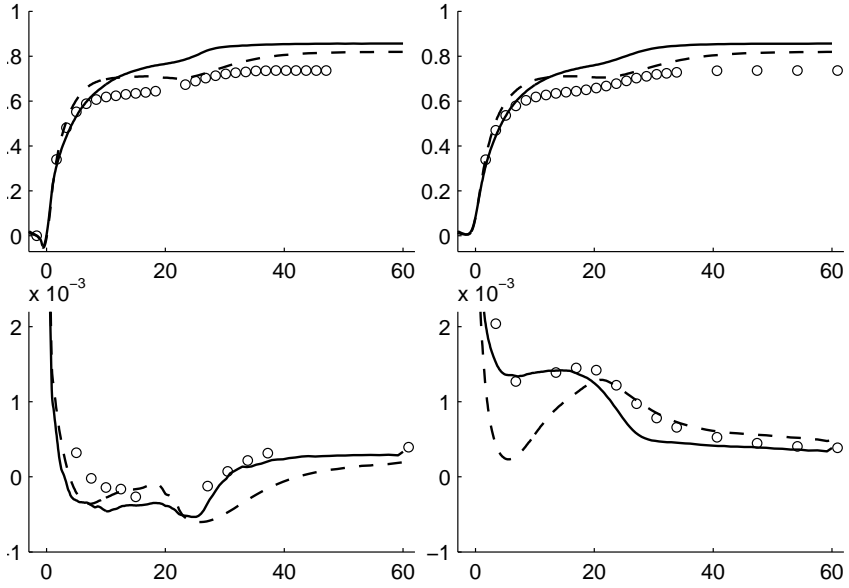


Figure 17: Diffuser flow. C_p (top figures) and C_f (figures below) on the bottom wall (left figures) and top wall (right figures). Solid line: hybrid RANS/LES with turbulent interface condition; dashed line: RANS-like computation.

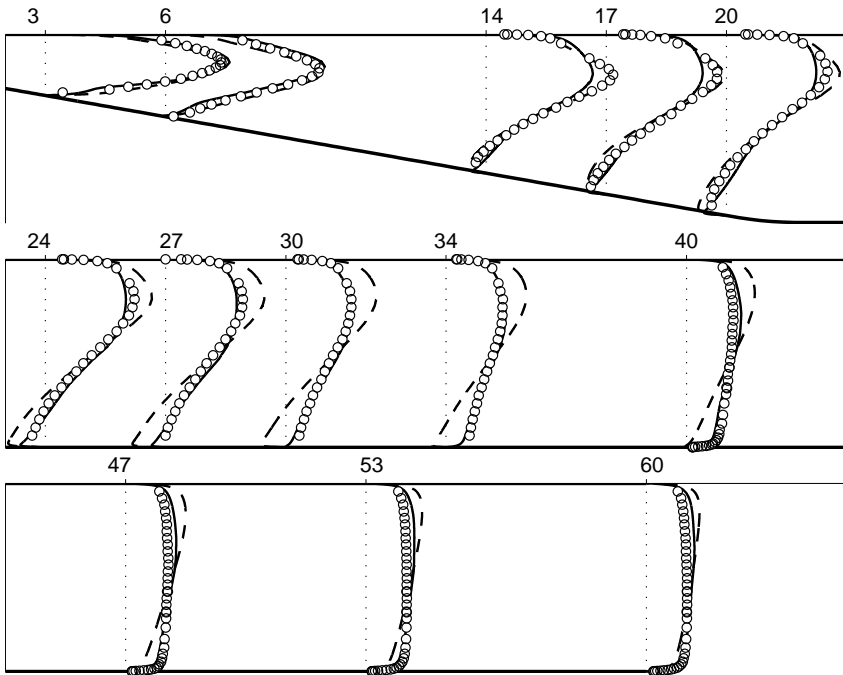


Figure 18: Diffuser flow. Velocities, $\langle \bar{U} \rangle$. Solid line: hybrid RANS/LES with turbulent interface condition; dashed line: RANS-like computation.

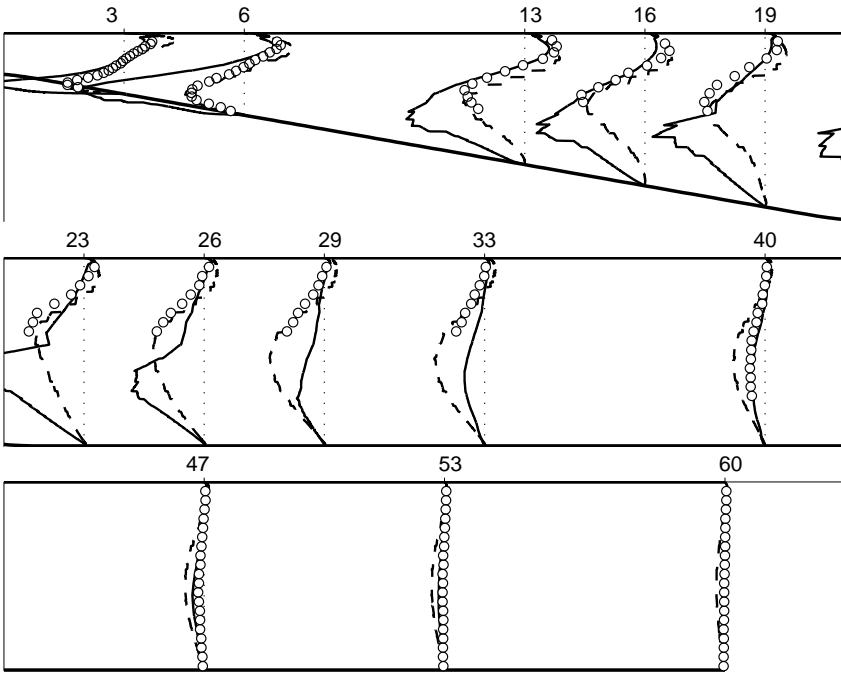


Figure 19: Diffuser flow. Resolved and modelled shear stresses, $-\langle uv \rangle$. Solid line: hybrid RANS/LES with turbulent interface condition; dashed line: RANS-like computation.

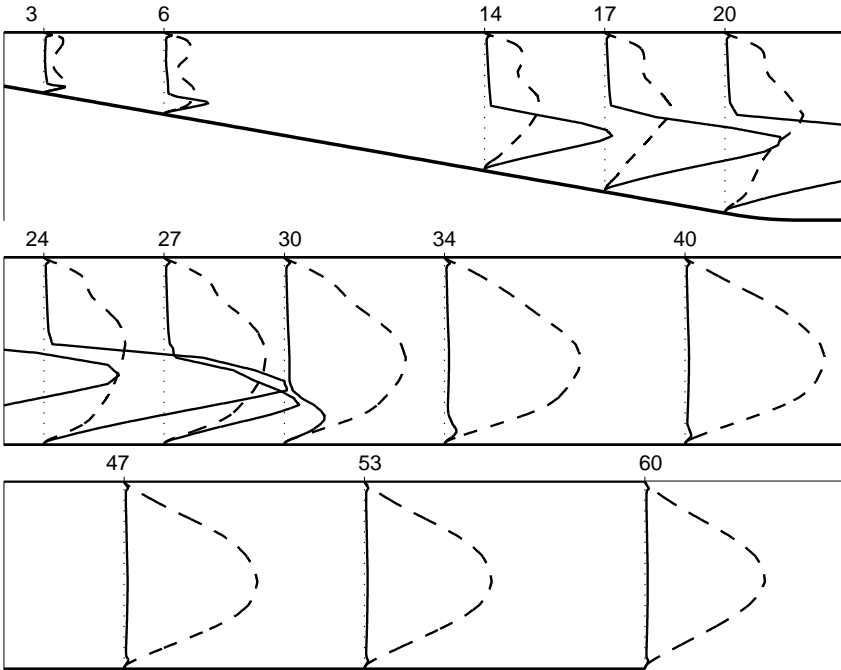


Figure 20: Diffuser flow. Eddy viscosities. Solid line: hybrid RANS/LES with turbulent interface condition; dashed line: RANS-like computation.

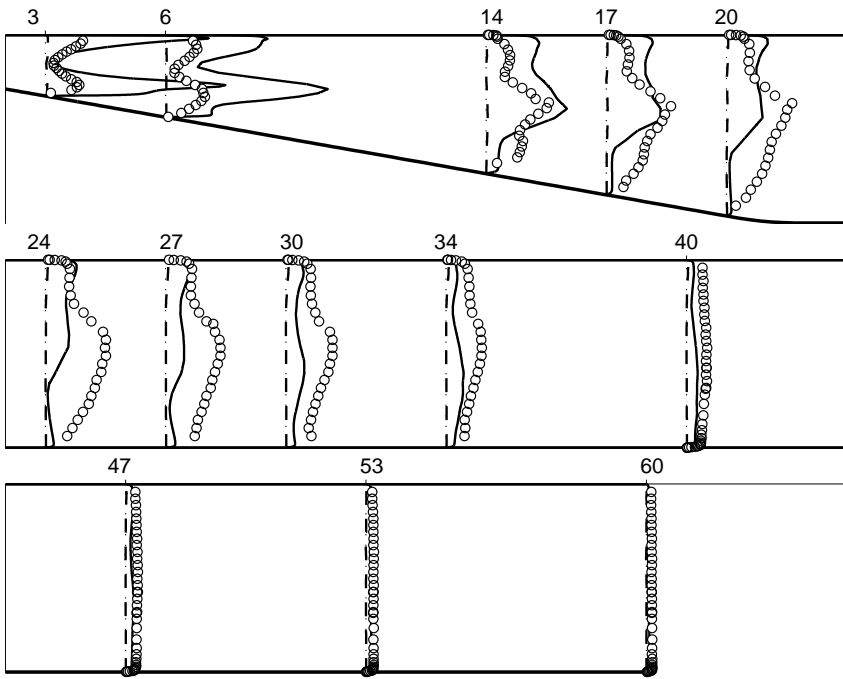


Figure 21: Diffuser flow. Resolved $\langle \overline{uu} \rangle$ stresses. Solid line: hybrid RANS/LES with turbulent interface condition; dashed line: RANS-like computation.

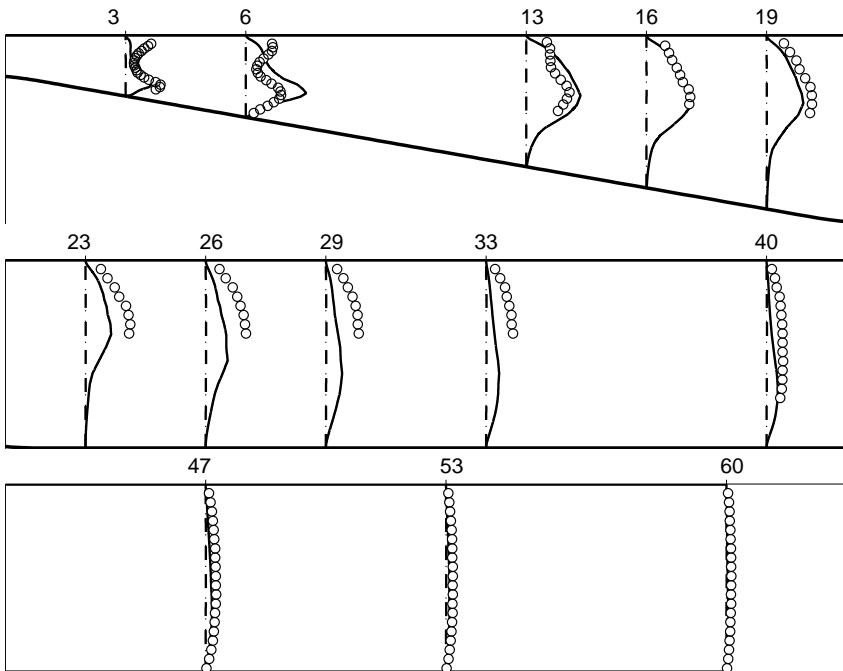


Figure 22: Diffuser flow. Resolved $\langle \overline{vv} \rangle$ stresses. Solid line: hybrid RANS/LES with turbulent interface condition; dashed line: RANS-like computation.

Appendix

Smooth one-equation model

In most of our hybrid RANS/LES computations the k -equation RANS model is switched abruptly to the SGS model at a prescribed node away from the wall (the matching line). This leads to a discontinuity at the matching line. We are able to smooth out this transition between the two models by using the model described in Table 2.

	Smoothed model
C_ε	$1.025 + 0.025 \tanh\left(\frac{b}{y_{ml}}(y - y_{ml})\right)$
C_k	$0.08 - 0.01 \tanh\left(\frac{b}{y_{ml}}(y - y_{ml})\right)$
ℓ_ε	$\ell_\Delta \tanh(\ell_{\varepsilon i}/\ell_\Delta)$
ℓ_k	$\ell_\Delta \tanh(\ell_{k i}/\ell_\Delta)$

where

$$\begin{aligned}\ell_{\varepsilon i} &= 2.495 \cdot y(1 - e^{-0.2 \cdot y \cdot \sqrt{k}/\nu}) \\ \ell_{k i} &= 2.495 \cdot y(1 - e^{-0.0143 \cdot y \cdot \sqrt{k}/\nu}) \\ \ell_\Delta &= \frac{\Delta + \ell_0}{2} + \frac{\Delta - \ell_0}{2} \tanh\left(\frac{b}{y_{ml}}(y - y_{ml})\right)\end{aligned}$$

Table 2: The smoothed one-equation model.

Here the length scale in the RANS region is limited by an eddy-viscosity limiter (proposed by Johnston [24]), $\ell_0 = 0.085\delta/C_\mu^{3/4}$, where δ is the boundary layer thickness or as in the diffuser case the distance from the wall to the centre line and $C_\mu = 0.09$. The blending factor, b , is set to 3, which means that the blending starts at approximately $y = 2y_{ml}/3$ and ends at approximately $4y_{ml}/3$ (see Fig. 1). With this model the matching line, y_{ml} , could either be explicitly set, at e.g. a prescribed node or at certain wall distance, or implicitly set to $\Delta/2.495$, i.e. the length scale in the RANS region never exceeds the length scale in the LES region.

RANS-like results on the diffuser flow

In Figs. 23 and 24 results are shown from computations where the smooth model shown in Table 2 is used. Here the resolved stresses are close to zero and these results regard RANS-like simulations and

RANS-modelling issues. The "filter widths" shown in Fig. 23 are:

$$\Delta = \max(\Delta x, \Delta y, \Delta z, 0.085\delta/0.09^{3/4})$$

$$\Delta = \max(\Delta x, \Delta y, \Delta z, 0.085\delta/0.08^{3/4})$$

$$\Delta = \max(\Delta x, \Delta y, \Delta z, 0.085\delta/0.07^{3/4})$$

$$\Delta = \max(\Delta x, \Delta y, \Delta z, 0.085\delta/0.09^{3/4} \cdot 0.09/0.07)$$

$$\Delta = 0.085\delta/0.08^{3/4} + 3 \cdot \max(0.264 \cdot \Delta x, 0)$$

The matching line distance, y_{ml} , is set to $\Delta/2.495$ for all of these computations.

With the modification of the filter width in the outlet channel, applied on the computation shown with a thick line, the redevelopment of the boundary layer is slightly improved in the outlet channel.

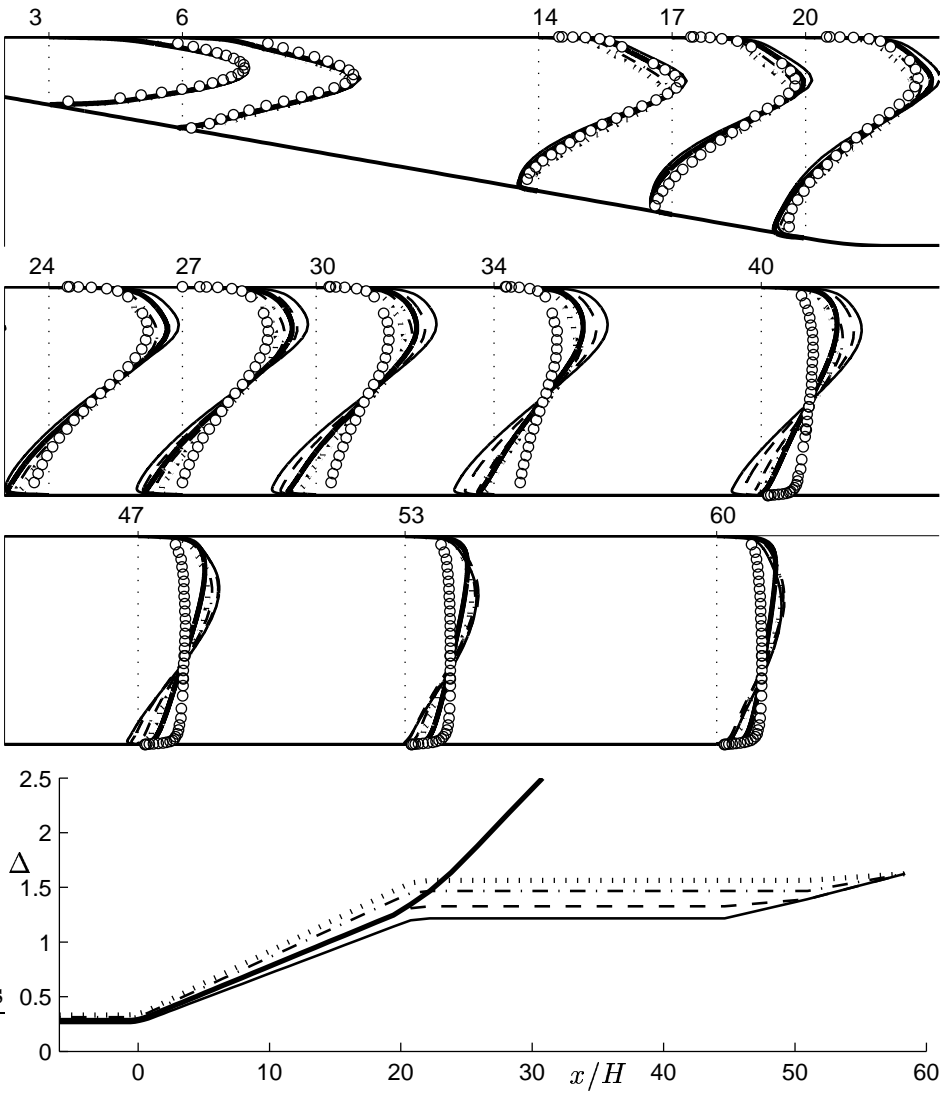


Figure 23: Diffuser flow. Averaged $\langle \bar{U} \rangle$ velocities. The difference between the computations are shown in the bottom figure, where the filter widths in the LES region are shown.

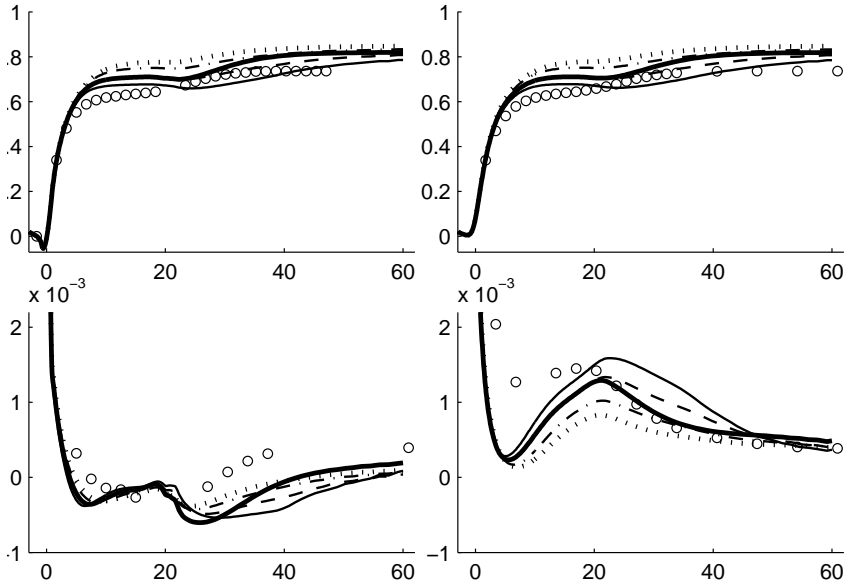


Figure 24: Diffuser flow. C_p (top figures) and C_f (figures below) on the bottom wall (left figures) and top wall (right figures). Same computations as described in Fig. 23.

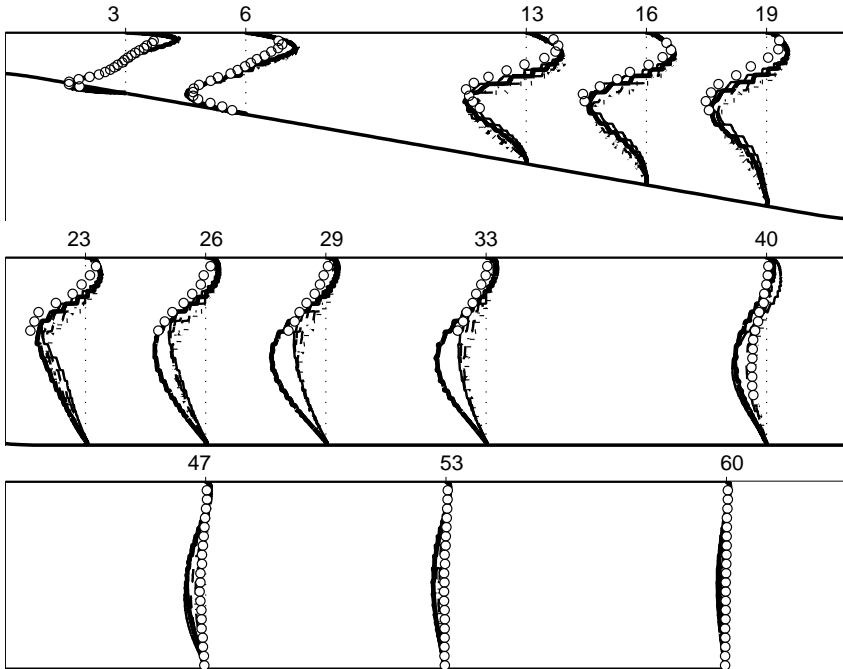


Figure 25: Diffuser flow. Modelled shear stresses (resolved stresses ≈ 0). Same computations as described in Fig. 23.

References

- [1] I. Mary and P. Sagaut. Large Eddy Simulation of flow around an airfoil near stall. *AIAA Journal*, 40(6):1139–1145, 2002.
- [2] H.-J. Kaltenbach, M. Fatica, R. Mittal, T.S. Lund, and P. Moin. Study of flow in a planar asymmetric diffuser using large-eddy simulation. *J. Fluid Mech.*, 390:151–185, 1999.
- [3] P.R. Spalart, W-H. Jou, M. Strelets, and S.R. Allmaras. Comments on the feasibility of LES for wings, and on a hybrid RANS/LES approach. 1st AFOSR Int. Conf. on DNS/LES, Aug. 4-8, 1997, Ruston, LA. In *Advances in DNS/LES*, C. Liu & Z. Liu Eds., Greyden Press, Columbus, OH, 1997.
- [4] M. Shur, P. R. Spalart, M. Strelets, and A. Travin. Detached-eddy simulation of an airfoil at high angle of attack. In W. Rodi and D. Laurence, editors, *Engineering Turbulence Modelling and Experiments 4*, pages 669–678. Elsevier Science, 1999.
- [5] M. Strelets. Detached eddy simulation of massively separated flows. 39th Aerospace Sciences Meeting, AIAA Paper 2001-0879, Reno, 2001.
- [6] S. Krajnović. *Large-Eddy Simulations for Computing the Flow Around Vehicles*. PhD thesis, Dept. of Thermo and Fluid Dynamics, Chalmers University of Technology, Gothenburg, 2002.
- [7] N. V. Nikitin, F. Nicoud, B. Wasistho, K. D. Squires, and P. R. Spalart. An approach to wall modeling in large-eddy simulations. *Physics of Fluids*, 12:1629–1632, 2000.
- [8] L. Davidson. Hybrid LES-RANS: A combination of a one-equation SGS model and a $k - \omega$ model for predicting recirculating flows. In *ECCOMAS CFD Conference*, Swansea, U.K., 2001.
- [9] L. Davidson and S.-H. Peng. Hybrid LES-RANS: A one-equation SGS model combined with a $k - \omega$ model for predicting recirculating flows (to appear). *International Journal for Numerical Methods in Fluids*, 2003.
- [10] P. Tucker and L. Davidson. Zonal k-l based large eddy simulations. AIAA paper 2003-0082, Reno, 2003.

- [11] H. Werner and H. Wengle. Large-eddy simulation of turbulent flow over and around a cube in a plane channel. In *9th Symp. Turbulent Shear Flows*, München, Germany, 1991.
- [12] L. Davidson, D. Cokljat, J. Fröhlich, M. Leschziner, C. Mellen, and W. Rodi, editors. *LESFOIL- Large Eddy Simulation of Flow Around a High-Lift Airfoil*. Springer, 2002. In print.
- [13] S. Dahlström and L. Davidson. Large Eddy Simulation of the Flow around an Aerospaciale A-Aerofoil. In *ECCOMAS 2000, European Congress on Computational Methods in Applied Sciences and Engineering, 11-14 September*, Barcelona, Spain, 2000.
- [14] S. Dahlström and L. Davidson. Large eddy simulation of the flow around an airfoil. 39th Aerospace Sciences Meeting, AIAA Paper 2001-0425, Reno, 2001.
- [15] J. S. Baggett. Some modeling requirements for wall models in large eddy simulation. In *Annual Research Briefs 1997*, pages 123–134, Center for Turbulent Research, Stanford Univ./NASA Ames Research Center, 1997.
- [16] P. Batten, U. Goldberg, and S. Chakravarthy. Using synthetic turbulence to interface RANS and LES. 41st Aerospace Sciences Meeting, AIAA Paper 2003-0081, Reno, 2003.
- [17] F. Hamba. An attempt to combine large eddy simulation with the $k - \varepsilon$ model in a channel-flow calculation. *Theoretical and Computational Fluid Dynamics*, 14:323–336, 2001.
- [18] L. Temmermann, M.A. Leschziner, and K. Hanjalić. A-priori studies of near-wall RANS model within a hybrid LES/RANS scheme. In W. Rodi and N. Fueyo, editors, *Engineering Turbulence Modelling and Experiments 5*, pages 17–326. Elsevier, 2002.
- [19] A. Yoshizawa. Statistical theory for compressible shear flows with the application of subgrid modelling. *Physics of Fluids A*, 29:2152–2163, 1986.
- [20] H.C. Chen and V.C. Patel. Near-wall turbulence models for complex flows including separation. *AIAA Journal*, 26:641–648, 1988.
- [21] C. Fureby. Large eddy simulation of rearward-facing step flow. *AIAA Journal*, 37(11):1401–1410, 1999.

- [22] 8th ERCOFTAC/IAHR/COST workshop on refined turbulence modelling. In *June 17-18, Helsinki University of Technology, Helsinki, Finland, 1999*.
- [23] P. Emvin. *The Full Multigrid Method Applied to Turbulent Flow in Ventilated Enclosures Using Structured and Unstructured Grids*. PhD thesis, Dept. of Thermo and Fluid Dynamics, Chalmers University of Technology, Gothenburg, 1997.
- [24] L.J. Johnston. Solution of the Reynolds-averaged Navier-Stokes equations for transonic aerofoil flows. *The Aeronautical Journal*, pages 253–273, 1991.